

Supporting Information

Double-Core Nanowire Formation from α -Furil via Pressure-Induced Planarization Pathway

Samuel G. Dunning,^{*a,b} Anirudh Hari,^a Li Zhu,^c Bo Chen,^{d,e} George D. Cody,^a Sebastiano Romi,^a Dongzhou Zhang^f and Timothy A. Strobel^{*a}

^a Earth and Planets Laboratory, Carnegie Institution for Science, Washington, District of Columbia 20015, United States

^b Division of Sciences and Mathematics, University of the District of Columbia, 4200 Connecticut Avenue NW, Washington, District of Columbia 20008, United States

^c Physics Department, Rutgers University-Newark, 101 Warren Street, Newark, NJ 07102, United States

^d Donostia International Physics Center, Paseo Manuel de Lardizabal, 4, 20018 Donostia-San Sebastian, Spain

^e IKERBASQUE, Basque Foundation for Science, Plaza Euskadi 5, 48009 Bilbao, Spain

^f Hawaii Institute of Geophysics and Planetology, School of Ocean and Earth Science and Technology, University of Hawaii at Manoa, Honolulu, HI 96822, United States

Correspondence should be addressed to samuel.dunning@udc.edu and tstrobel@carnegiescience.edu.

Contents

Materials and Experimental Methods	3
Theoretical Calculation Methods	4
Figure S1. In situ XRD patterns (with background correction) for a powder sample of α -furil, collected between 0 – 25.2 GPa ($\lambda = 0.4340 \text{ \AA}$) without a pressure transmitting medium (i.e., under anisotropic conditions). Data is reported in both d-space (left) and 2θ (right). Red asterisks indicate peaks corresponding to high pressure, <i>trans</i> -planar phase of α -furil with emerge at 1.9 GPa and persist until the onset of nanothread formation at 10.1 GPa. Green asterisks indicate peaks corresponding to the resulting nanothread polymer. Black dots represent diffraction from the Au pressure medium.	5
Table S1. Comparison of the cell parameters for the three high-pressure phases of α -furil collected at 0.5, 1.6, and 4.4 GPa respectively.....	5
Figure S2. Top: In situ FTIR absorbance spectra of α -furil showing data between $3600 - 2700 \text{ cm}^{-1}$ (left) and $1800 - 500 \text{ cm}^{-1}$ (right) collected during compression from 0 - 19.6 GPa. Red asterisks indicate new peaks corresponding to the high-pressure phase of α -furil (Phase II), green asterisks indicate new peaks which emerge after the onset of nanothread formation. The region between $2700 - 1800 \text{ cm}^{-1}$ has been omitted for clarity due to diamond interference. Bottom: In situ FTIR absorbance spectral of α -furil showing data between $1800 - 600 \text{ cm}^{-1}$ collected during compression and decompression between 0 - 4.6 GPa, demonstrating the reversibility of the transformation between Phase I and Phase II.	6
Figure S3. Top, left: In situ Raman spectra ($480 - 830 \text{ nm}$, $\lambda_{\text{ex}} = 532 \text{ nm}$) of α -furil collected upon compression from 0 – 18.2 GPa. Note the emergence of intense background emission at <i>ca.</i> 541 nm above 3.3 GPa. Top, right: In situ Raman spectra (-500 to 2000 cm^{-1} , $\lambda_{\text{ex}} = 532 \text{ nm}$) of α -furil collected upon compression from 0 – 3.3 GPa. Red asterisks above 1.1 GPa indicate new vibrational modes which emerge as a result of the transition to the <i>trans</i> -planar phase of α -furil. Blue asterisks at 0 cm^{-1} and $\sim 1343 \text{ cm}^{-1}$ represent the laser line and diamond emission respectively. Bottom: Comparison of the Raman spectra ($480 - 830 \text{ nm}$, $\lambda_{\text{ex}} = 532 \text{ nm}$) of α -furil compressed to 18.2 GPa and the recovered nanothreads at ambient pressure, indicating that the new, broad emission at <i>ca.</i> 623 nm is representative of the new nanothread polymer. Spectra are normalized for collection time.	7
Figure S4. Left: Comparison of XRD patterns collected on recovered samples of α -furil nanothreads synthesized using a diamond anvil cell (DAC, black, $\lambda = 0.4340 \text{ \AA}$) and a Paris-Edinburgh (PE) press (red, $\lambda = 1.5406 \text{ \AA}$). Both samples were compressed without pressure transmitting medium. Right: Comparison of FTIR spectra of recovered samples of α -furil nanothreads synthesized using a diamond anvil cell (DAC, black) and a Paris-Edinburgh (PE) press (red). Here, the DAC sample was compressed using KBr as the pressure transmitting medium and the PE press sample was compressed without a pressure transmitting medium.	8
Figure S5. Thermogravimetric analysis (TGA, dark lines) and differential scanning calorimetry (DSC, faint lines) curves for α -furil (black) and the recovered nanothread product (red), collected between $50 - 1000 \text{ }^\circ\text{C}$. Dotted lines indicate the onset of decomposition in TGA curves. Exothermic transitions are represented in the DSC curves by an increase in heat flow, endothermic transitions are represented by a decrease. Note that the noise in the α -furil data is due to sublimation of sample and contamination of the reference pan. Accordingly, data collected above $215 \text{ }^\circ\text{C}$ has been omitted.	9

Table S2. Comparison of relative energies for individual nanothreads and packed crystal structures of four candidate nanothread structures of the high-pressure polymerization product of α -fural. All structures were optimized using VASP DFT, and all energies are reported as relative to structure A.	10
Table S3. Cell parameters obtained from the Rietveld optimization of candidate nanothread structure C (see Table S2), calculated from PXRD data collected upon recovery to ambient.	10
Table S4. Atomic coordinates obtained from the Rietveld optimization of candidate nanothread structure C (see Table S2). Note: Due to the breadth of peaks in the recovered sample there is some uncertainty in the precise atomic positions. The thermal parameter, B, was refined with all atoms treated as equivalent. H atoms were placed 1 Å away from the nearest neighbor atom.	11
Figure S6. Images of first-principles molecular dynamics simulations of α -fural carried out at 50 GPa and 500 K. Snapshots are taken at 0, 100, 150, 200, 300 and 400 fs and show the onset of a pressure-induced reaction between fural molecules, beginning with a series of cascade, carbon-only [4+2] cycloaddition reactions, followed by reaction between carbonyl groups in the 1,2-diketone bridge.	11
Figure S7. Comparison of the experimental FTIR spectrum for a washed sample of α -fural (black), collected between 500 – 3600 cm^{-1} with calculated IR spectra for each candidate nanothread structure (red). Calculated frequencies, shown by arbitrary Lorentzian peak widths have not been scaled to match with experimental data and are presented as calculated. Insets: Visualization of the structure of the nanothread structure used to generate the calculated data shown.	12
References.	13

Materials and Experimental Methods.

Materials. α -Furil (2,2'-Furil, >98%, TCI America, LOT #: 4TIDF) and dichloromethane (DCM, 99.9%; Sigma-Aldrich) were used as received without further purification.

High Pressure Synthesis. Diamond anvil cells (DACs) containing type I diamonds with 400 μm culets were used for all XRD measurements, type IIa diamonds of the same size were used for all FTIR/Raman measurements. Re gaskets were pre-indented to ca. 40 μm before a ca. 180 μm hole was drilled through the center of the indentation. The hole in the Re gasket was used as the sample chamber. For in-situ FTIR/Raman measurements a ruby chip was added with the sample for in situ measurement of pressure within the DAC, estimated through ruby fluorescence.^{1,2} For in situ XRD measurements gold (Au) was added to the sample for in situ measurement of pressure using the Au equation of state. Powder or single crystal samples of α -furil were loaded directly into the sample chamber. Powder measurements were conducted without any additional pressure transmitting medium, single crystal studies were carried out using $\text{Ne}_{(\text{g})}$ as a pressure transmitting medium.

Paris-Edinburgh (PE) press experiments were carried out using a VX3 Paris-Edinburgh press equipped with double-toroidal sintered diamond anvils. A Teledyne ISCO 30D Syringe Pump with a maximum pressure of 207 MPa was used to drive the system. Samples were synthesized by packing powders of α -furil into a Ti (ELI grade) sample chamber and were pressurized to a set pressure, with the rate of pressurization set by the flow rate. Samples were held at the desired pressure for 24 hours before decompression. The rate of compression and decompression are as follows: 1 mL/min below 7 MPa, 0.3 mL/min from 7 to 34 MPa, 0.02 mL/min from 34 to 138 MPa, 0.01 mL/min from 138 to 165 MPa.

Nanothread Purification. PE Press samples were recovered from their Ti gaskets and suspended in an excess of dichloromethane (2 mL). The samples were thoroughly sonicated using a Branson 200 Ultrasonic Cleaner. The samples were recovered by centrifugation using an IEC Centra CL2 and the supernatant was removed. This process was carried out in triplicate, and samples were placed in a Fisher Scientific Isotemp 282A oven set to 120 °C to dry.

X-ray Diffraction. In situ synchrotron X-ray diffraction (XRD) was measured at the 13-BM-C beamline at the Advanced Photon Source, Argonne National Laboratory. Calibration was performed using a LaB_6 standard. Data was collected using a monochromatic beam ($\lambda = 0.4340 \text{ \AA}$). Powder samples were scanned over a rotation range of $\omega \pm 2^\circ$. Single crystal samples were scanned over a range of $\omega \pm 33^\circ$ with a step size of 0.5° . To account for the limited opening window caused by the DAC, multiple crystals in different orientations were loaded into the same cell, and their respective diffraction frames were analyzed and merged during data processing to improve overall coverage and completion. $\text{Au}_{(\text{s})}$ and $\text{Ne}_{(\text{g})}$ were used as pressure references for powder and single-crystal diffraction studies.

Diffraction patterns for recovered Paris-Edinburgh (PE) Press samples were collected using either a Bruker D2 PHASER ($\lambda = 1.5406 \text{ \AA}$) equipped with a LYNXEYE 1D detector, or a Bruker D8 diffractometer ($\lambda = 1.5406 \text{ \AA}$) equipped with a 2mm collimator and VÅNTEC-500 area detector. Refinement of powder X-ray diffraction data was performed using the JADE software suite.

Vibrational Spectroscopy. Fourier-transform infrared (FTIR) spectra were obtained using a Bruker Vertex spectrometer with Hyperion microscope with MCT detector. The total spectral range spanned 500 to 8,300 cm^{-1} with a resolution of 4 cm^{-1} . In situ high-pressure measurements were referenced to transmission through the diamond anvils at ambient. The intrinsic diamond absorption has been removed for clarity. The recovered sample was referenced to open air. Ruby powder was used as the pressure calibrant.

Raman spectra were collected with a Princeton Instruments spectrograph SP2750 with a 750 mm focal length. The system was equipped with a 532 nm diode laser, which was focused through a 20 \times long working distance objective lens. Raman light was collected in the backscatter geometry through a 50 μm confocal pinhole. Raman light was collected through a 50 μm slit and dispersed off either a 300 or 1800 $\text{g}\cdot\text{mm}^{-1}$ grating onto a $\text{N}_2(\text{l})$ cooled charge coupled device detector. The spectrometer was calibrated by measuring the emission lines of Ne.

Nuclear Magnetic Resonance. Samples were loaded into a 5 mm OD zirconia rotor and spun at the magic angle at 11.5 kHz. The ^{13}C solid state NMR spectra were acquired using Variable Amplitude (on the ^{13}C channel) ^1H - ^{13}C Cross Polarization (VACP) NMR with a contact time of 4.5 ms. As each of the carbon positions have different CP dynamical parameters (e.g., T_{CH} and $T_{1\rho}$) peak intensities are not proportional to concentration. The VACP NMR

spectrum solely reports the frequencies of the carbon nuclei. A $3\pi/2$ pulse sequence was used to suppress ^{13}C background signal from outside the rotor. NMR data was fit using the fityk software suite.

Thermogravimetric Analysis/Differential Scanning Calorimetry. Thermogravimetric analysis (TGA) and differential scanning calorimetry measurements were collected using a TA Instruments SDT-650 TGA/DSC. Experiments were carried out under inert Ar atmosphere with a flow rate of 100 mL/min. Samples were heated between 50 – 1000 °C after equilibration at 50 °C with a ramp rate of 10 °C/min.

Theoretical Calculation Methods.

Structural Optimization and FTIR Calculations. Ab initio Molecular Dynamics (MD) simulations and structure optimizations were carried out using density functional theory (DFT) within the Perdew-Burke-Ernzerhof parametrization³ of generalized gradient approximation⁴ and the nonlocal van der Waals density functional (vdW-DF)^{5,6} as implemented in the VASP (Vienna Ab Initio simulation package) code⁷. The all-electron projector augmented wave (PAW) pseudopotentials⁸ with $2s^22p^2$, $2s^22p^4$, and $1s^1$ electrons as valence for C, O, and H, respectively, was adopted. The energy cutoff 520 eV and appropriate Monkhorst-Pack k meshes⁹ were chosen to ensure that enthalpy calculations are well converged to better than 1 meV/formula unit. All structures were relaxed with the force convergence tolerance set to 0.01 eV/Å. Using these relaxed structures, density-functional perturbation theory (DFPT) calculations were performed with VASP^{20,10} to determine the IR frequencies and associated intensities.

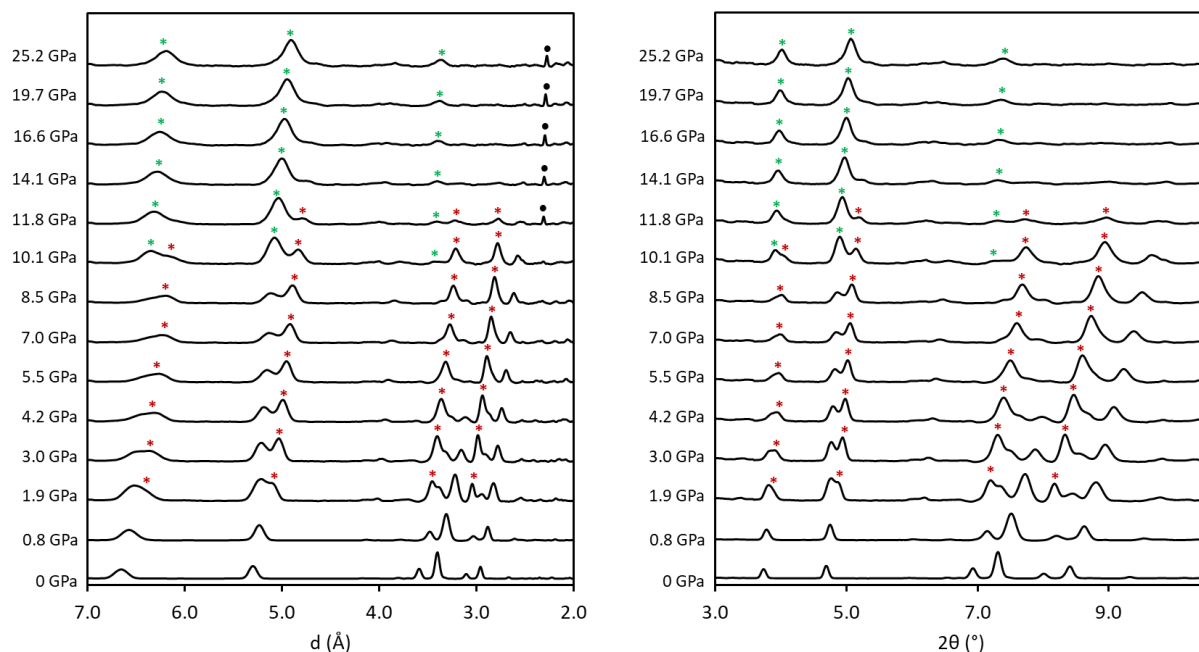


Figure S1. In situ XRD patterns (with background correction) for a powder sample of α -furil, collected between 0 – 25.2 GPa ($\lambda = 0.4340 \text{ \AA}$) without a pressure transmitting medium (i.e., under anisotropic conditions). Data is reported in both d-space (left) and 2θ (right). Red asterisks indicate peaks corresponding to high pressure, *trans*-planar phase of α -furil with emerge at 1.9 GPa and persist until the onset of nanothread formation at 10.1 GPa. Green asterisks indicate peaks corresponding to the resulting nanothread polymer. Black dots represent diffraction from the Au pressure medium.

Table S1. Comparison of the cell parameters for the three high-pressure phases of α -furil collected at 0.5, 1.6, and 4.4 GPa respectively.

Pressure (GPa)	Space Group	a (Å)	b (Å)	c (Å)	B (°)	Volume (Å ³)
0.5	<i>Fdd2</i>	14.6170(9)	30.092(12)	3.6052(3)	90	1585.7(7)
1.6	<i>P2₁/n</i>	14.586(5)	7.0535(14)	3.4512(6)	93.132(15)	354.55(16)
4.4	<i>P2₁/n</i>	14.228(16)	6.957(7)	3.313(3)	94.48(3)	326.9(6)

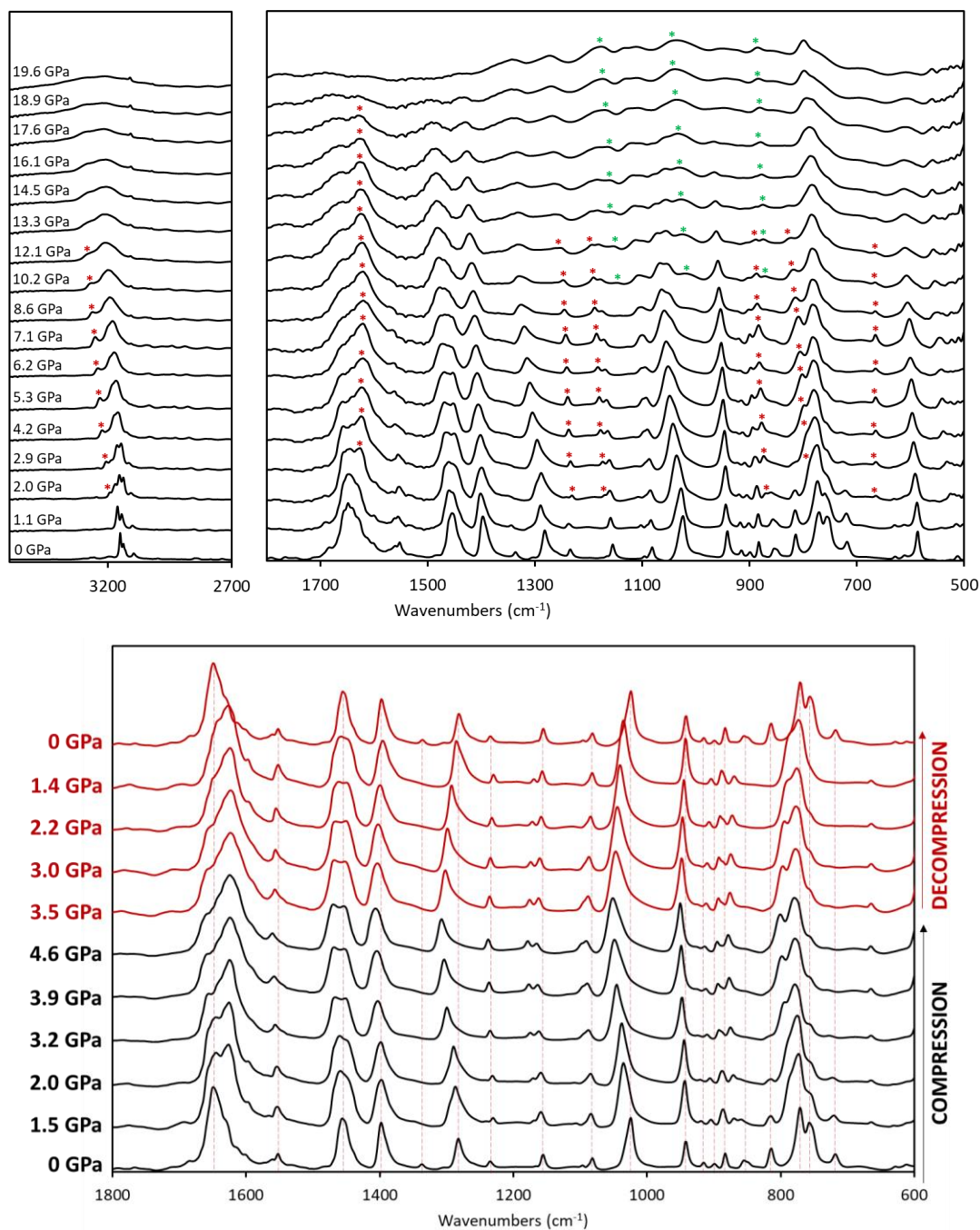


Figure S2. Top: In situ FTIR absorbance spectra of α -furil showing data between 3600 – 2700 cm^{-1} (left) and 1800 – 500 cm^{-1} (right) collected during compression from 0 - 19.6 GPa. Red asterisks indicate new peaks corresponding to the high-pressure phase of α -furil (Phase II), green asterisks indicate new peaks which emerge after the onset of nanothread formation. The region between 2700 – 1800 cm^{-1} has been omitted for clarity due to diamond interference. Bottom: In situ FTIR absorbance spectral of α -furil showing data between 1800 – 600 cm^{-1} collected during compression and decompression between 0 - 4.6 GPa, demonstrating the reversibility of the transformation between Phase I and Phase II.

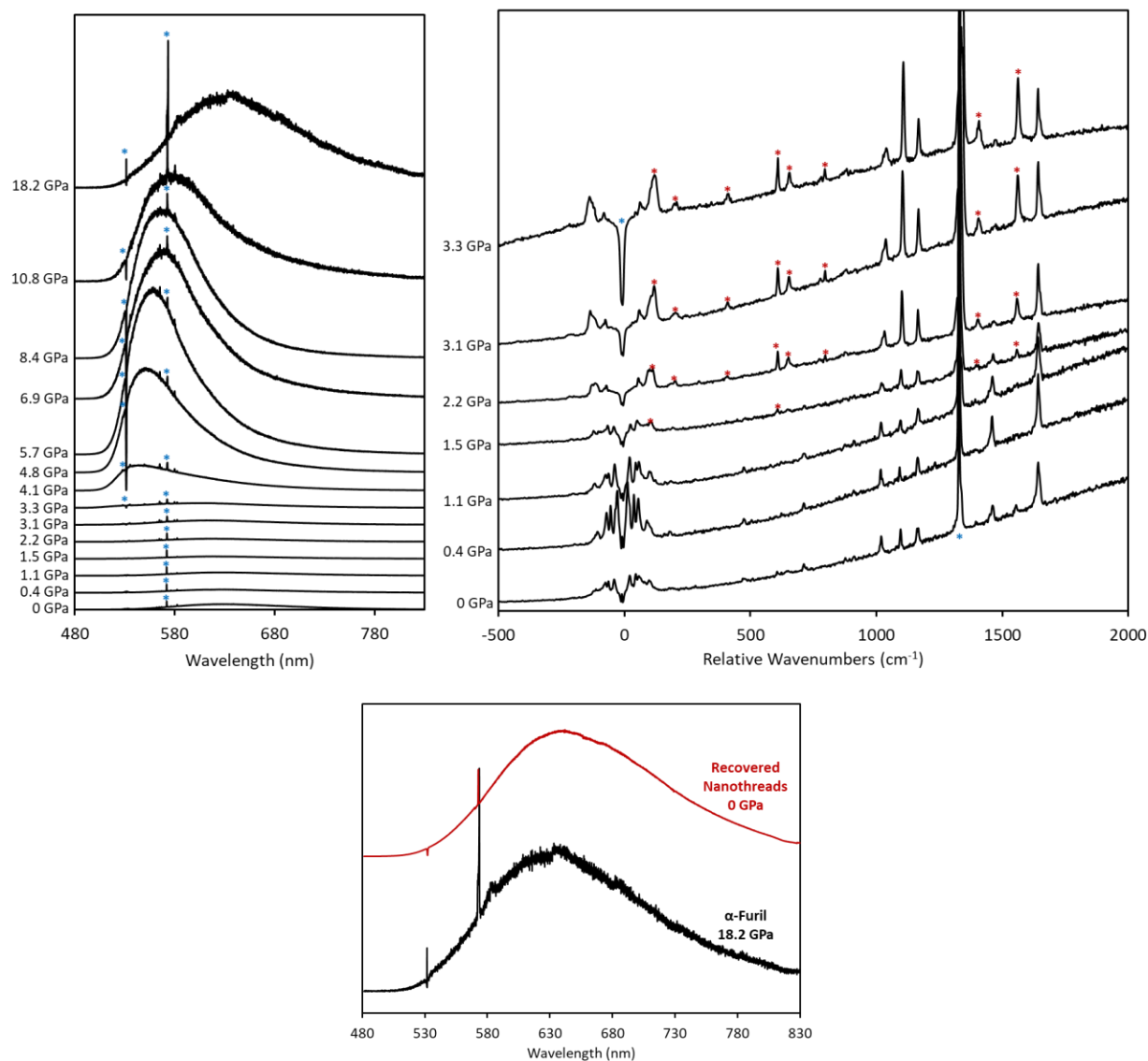


Figure S3. Top, left: In situ Raman spectra (480 - 830 nm, $\lambda_{\text{ex}} = 532$ nm) of α -furil collected upon compression from 0 – 18.2 GPa. Note the emergence of intense background emission at *ca.* 541 nm above 3.3 GPa. Top, right: In situ Raman spectra (-500 to 2000 cm^{-1} , $\lambda_{\text{ex}} = 532$ nm) of α -furil collected upon compression from 0 – 3.3 GPa. Red asterisks above 1.1 GPa indicate new vibrational modes which emerge as a result of the transition to the *trans*-planar phase of α -furil. Blue asterisks at 0 cm^{-1} and ~ 1343 cm^{-1} represent the laser line and diamond emission respectively. Bottom: Comparison of the Raman spectra (480 - 830 nm, $\lambda_{\text{ex}} = 532$ nm) of α -furil compressed to 18.2 GPa and the recovered nanothreads at ambient pressure, indicating that the new, broad emission at *ca.* 623 nm is representative of the new nanothread polymer. Spectra are normalized for collection time.

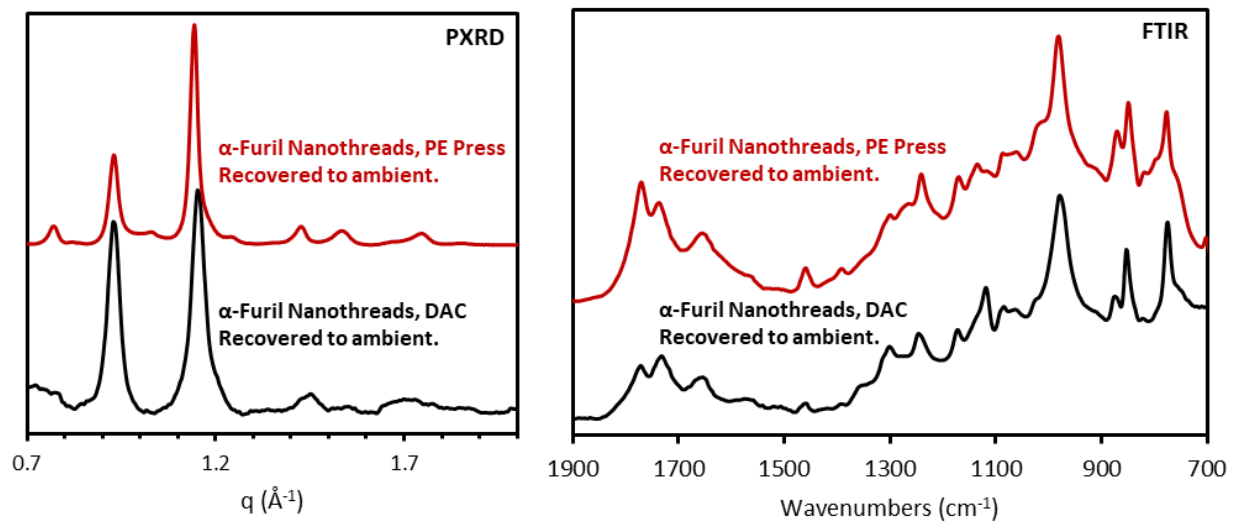


Figure S4. Left: Comparison of XRD patterns collected on recovered samples of α -furil nanothreads synthesized using a diamond anvil cell (DAC, black, $\lambda = 0.4340 \text{ \AA}$) and a Paris-Edinburgh (PE) press (red, $\lambda = 1.5406 \text{ \AA}$). Both samples were compressed without pressure transmitting medium. Right: Comparison of FTIR spectra of recovered samples of α -furil nanothreads synthesized using a diamond anvil cell (DAC, black) and a Paris-Edinburgh (PE) press (red). Here, the DAC sample was compressed using KBr as the pressure transmitting medium and the PE press sample was compressed without a pressure transmitting medium.

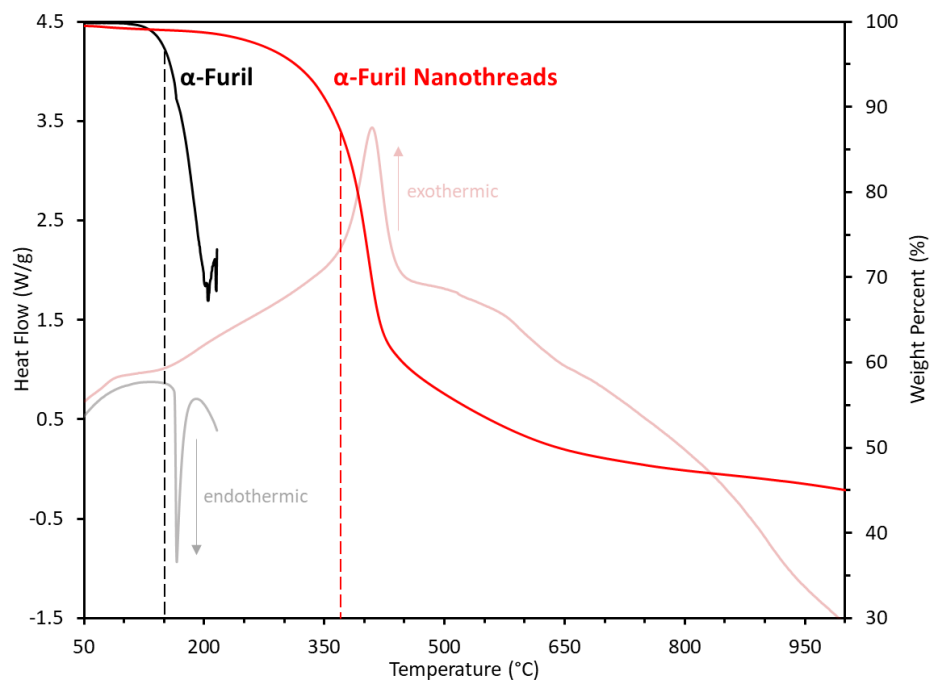


Figure S5. Thermogravimetric analysis (TGA, dark lines) and differential scanning calorimetry (DSC, faint lines) curves for α -furil (black) and the recovered nanothread product (red), collected between 50 – 1000 °C. Dotted lines indicate the onset of decomposition in TGA curves. Exothermic transitions are represented in the DSC curves by an increase in heat flow, endothermic transitions are represented by a decrease. Note that the noise in the α -furil data is due to sublimation of sample and contamination of the reference pan. Accordingly, data collected above 215 °C has been omitted.

Table S2. Comparison of relative energies for individual nanothreads and packed crystal structures of four candidate nanothread structures of the high-pressure polymerization product of α -fural. All structures were optimized using VASP DFT, and all energies are reported as relative to structure A.

Thread	A	B	C	D
$\Delta E/\text{molecule}$ (eV), single thread	0.00	+0.16	-0.10	+1.14
$\Delta E/\text{molecule}$ (eV), packed structures	0.00	+0.28	+0.04	+1.32

Table S3. Cell parameters obtained from the Rietveld optimization of candidate nanothread structure C (see Table S2), calculated from PXRD data collected upon recovery to ambient.

	Thread C
Formula	$(\text{C}_{10}\text{H}_6\text{O}_4)_n$
Space Group	$P2_1/n$
a (Å)	16.442(4)
b (Å)	7.436(3)
c (Å)	3.10(1)
β (°)	90.54(9)
Volume (Å³)	379.4(4)
Density (g/cm³)	1.66
R_{wp}	8.78%

Table S4. Atomic coordinates obtained from the Rietveld optimization of candidate nanothread structure C (see Table S2). Note: Due to the breadth of peaks in the recovered sample there is some uncertainty in the precise atomic positions. The thermal parameter, B, was refined with all atoms treated as equivalent. H atoms were placed 1 Å away from the nearest neighbor atom.

Atom	x	y	z	Occupancy	B
C1	0.5772(1)	0.7551(2)	0.977(2)	1	0.5
C2	0.6801(1)	0.8566(4)	0.420(1)	1	0.5
C3	0.5874(1)	0.7047(2)	0.535(1)	1	0.5
C4	0.5499(1)	0.5042(3)	0.514(2)	1	0.5
C5	0.6613(1)	0.8691(3)	0.957(1)	1	0.5
O1	0.32922(9)	0.3205(1)	0.6918(7)	1	0.5
O2	0.42816(7)	0.5773(2)	0.936(1)	1	0.5
H1	0.38058	0.93771	0.05596	1	---
H2	0.49387	0.8519	0.95881	1	---
H3	0.24032	0.10082	0.52714	1	---

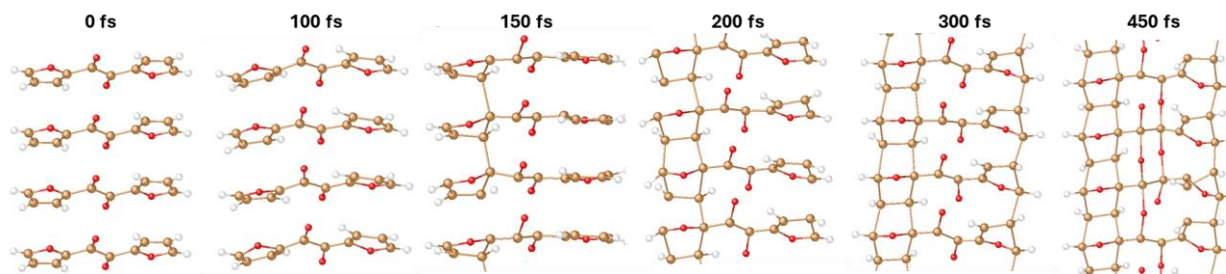


Figure S6. Images of first-principles molecular dynamics simulations of α -furil carried out at 50 GPa and 500 K. Snapshots are taken at 0, 100, 150, 200, 300 and 400 fs and show the onset of a pressure-induced reaction between furil molecules, beginning with a series of cascade, carbon-only [4+2] cycloaddition reactions, followed by reaction between carbonyl groups in the 1,2-diketone bridge.

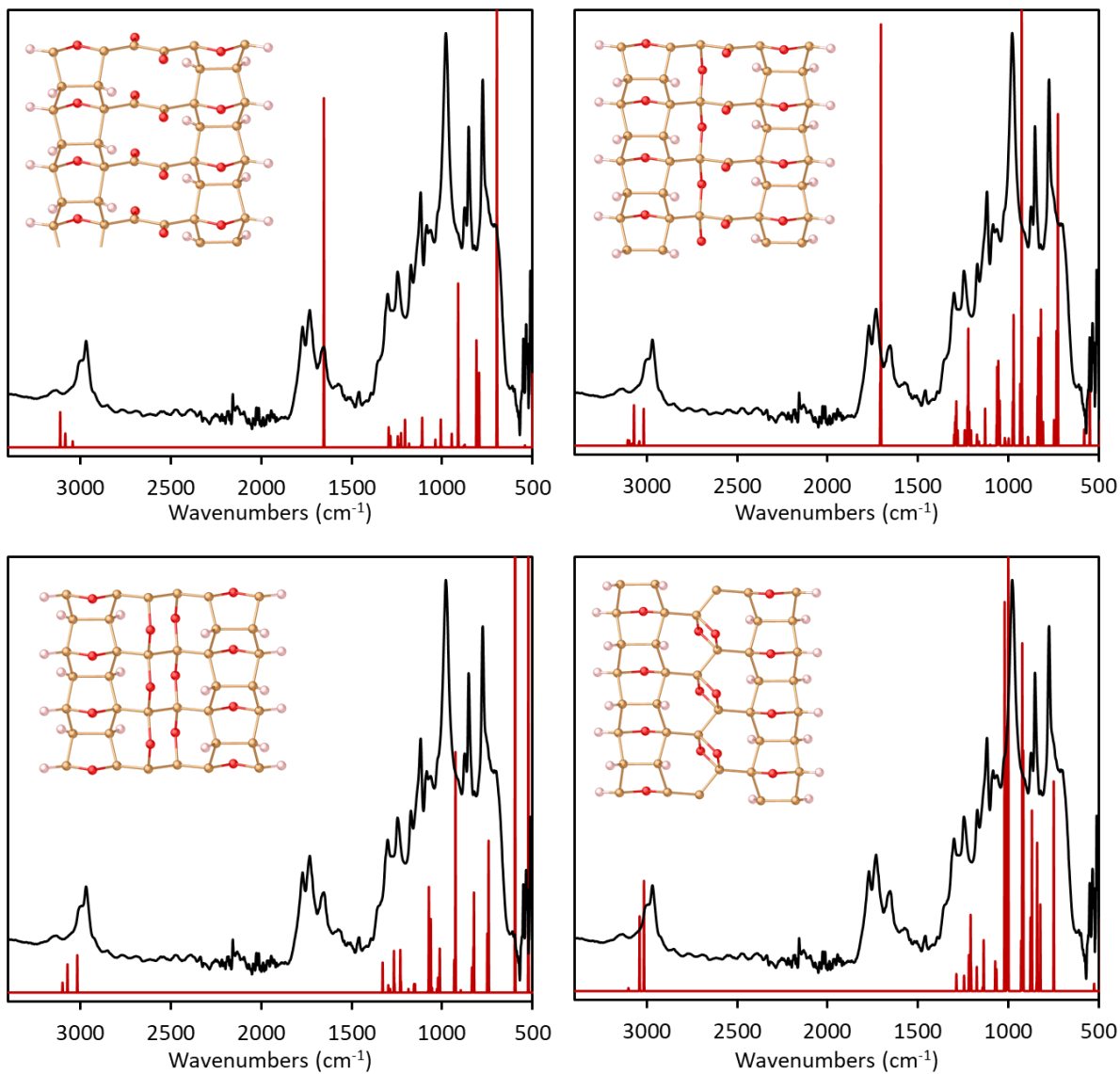


Figure S7. Comparison of the experimental FTIR spectrum for a washed sample of α -fural (black), collected between 500 – 3600 cm^{-1} with calculated IR spectra for each candidate nanowire structure (red). Calculated frequencies, shown by arbitrary Lorentzian peak widths have not been scaled to match with experimental data and are presented as calculated. Insets: Visualization of the structure of the nanowire structure used to generate the calculated data shown.

References.

- ¹ Dewaele, A.; Torrent, M.; Loubeyre, P.; Mezouar, M. *Physical Review B*, 2008, **78**, 104102.
- ² Mao, H. K.; Xu, J.; Bell, P. M. *Journal of Geophysical Research: Solid Earth*, 1986, **91**, 4673-4676.
- ³ Perdew, J. P.; Burke, K.; Ernzerhof, M. Generalized Gradient Approximation Made Simple. *Phys Rev Lett* 1996, **77** (18), 3865–3868. <https://doi.org/10.1103/physrevlett.77.3865>.
- ⁴ Perdew, J. P.; Wang, Y. Accurate and Simple Analytic Representation of the Electron-Gas Correlation Energy. *Phys Rev B* 1992, **45** (23), 13244–13249. <https://doi.org/10.1103/physrevb.45.13244>.
- ⁵ Sun, J.; Remsing, R. C.; Zhang, Y.; Sun, Z.; Ruzsinszky, A.; Peng, H.; Yang, Z.; Paul, A.; Waghmare, U.; Wu, X.; Klein, M. L.; Perdew, J. P. Accurate First-Principles Structures and Energies of Diversely Bonded Systems from an Efficient Density Functional. *Nat Chem* 2016, **8** (9), 831–836. <https://doi.org/10.1038/nchem.2535>.
- ⁶ Zhang, G.-X.; Tkatchenko, A.; Paier, J.; Appel, H.; Scheffler, M. Van Der Waals Interactions in Ionic and Semiconductor Solids. *Phys Rev Lett* 2011, **107** (24), 245501. <https://doi.org/10.1103/physrevlett.107.245501>.
- ⁷ Kresse, G.; Furthmüller, J. Efficient Iterative Schemes for Ab Initio Total-Energy Calculations Using a Plane-Wave Basis Set. *Phys Rev B* 1996, **54** (16), 11169–11186. <https://doi.org/10.1103/physrevb.54.11169>.
- ⁸ Blöchl, P. E. Projector Augmented-Wave Method. *Phys Rev B* 1994, **50** (24), 17953–17979. <https://doi.org/10.1103/physrevb.50.17953>.
- ⁹ Monkhorst, H. J.; Pack, J. D. Special Points for Brillouin-Zone Integrations. *Phys Rev B* 1976, **13** (12), 5188–5192. <https://doi.org/10.1103/physrevb.13.5188>.
- ¹⁰ Gajdoš, M.; Hummer, K.; Kresse, G.; Furthmüller, J.; Bechstedt, F. Linear Optical Properties in the Projector-Augmented Wave Methodology. *Phys Rev B* 2006, **73** (4), 045112. <https://doi.org/10.1103/physrevb.73.045112>.